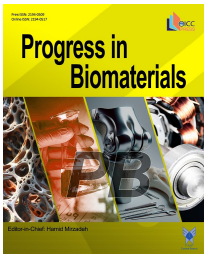

Prog. Biomater. 2026; 15(1) : 62-79

Progress in Biomaterials (PIBM)

https://doi.org/10.57647/pibm.2026.152604

Research Article

Sodium Alginate Encapsulated *Melissa officinalis* Extract using Nano Spray Drying: Characterization, and Release Studies

Leila Bagherpour[1], Samad Nejad Ebrahimi[1,*], Hasan Rafati[2], Marzieh Omrani[1]

[1]*Department of Phytochemistry, Medicinal Plants and Drugs Research Institute, Shahid Beheshti University, Tehran, Iran*
[2]*Department of Pharmaceutical Engineering, Medicinal Plants and Drugs Research Institute, Shahid Beheshti University, Tehran, Iran*

[*]**Corresponding author:** s_ebrahimi@sbu.ac.ir

Article History

Received:
15 December 2025

Revised:
13 March 2026

Accepted:
27 March 2026

Published in Issue:
31 March 2026

Abstract:

Polyphenols from *Melissa officinalis* exhibit notable antioxidant and therapeutic activities, yet their instability limits their practical application in food and pharmaceutical systems. Encapsulation with natural biopolymers offers a promising approach to improve stability, protect compounds from degradation, and support targeted delivery. This study developed a sodium-alginate encapsulation system to enhance the stability and enable controlled release of *M. officinalis* polyphenols. Encapsulated samples were produced using a fixed core-to-wall ratio through a nano spray-drying technique, and multiple drying conditions were optimized. The physicochemical and functional properties of the obtained encapsulated materials were analyzed using FTIR, DSC, particle size measurements, antioxidant assays, and *in vitro* release tests. The optimized formulation yielded uniform particles (~ 620 nm) with high encapsulation efficiency (88.65 ± 0.57%) and a loading capacity of 16.4%. Structural analyses verified the successful entrapment of phenolic compounds within the alginate matrix and confirmed enhanced thermal stability. *In vitro* release studies demonstrated pH-responsive behavior, with limited release in acidic conditions and near-complete release at intestinal pH. Molecular docking and dynamics simulations further indicated favorable interactions between rosmarinic acid and the alginate network. The findings demonstrate that nano spray-dried sodium alginate colloids provide an effective system for delivering polyphenols, supporting their potential use in functional food and pharmaceutical products.

Keywords: Polyphenol encapsulation; Controlled release; Antioxidant activity; Molecular docking

Cite this article: Bagherpour L, Nejad Ebrahimi S, Rafati H, Omrani M. Sodium Alginate Encapsulated *Melissa officinalis* Extract using Nano Spray Drying: Characterization, and Release Studies. Prog. Biomater., 2026;15(1): 62-79. https://doi.org/10.57647/pibm.2026.152604

1. Introduction

Melissa officinalis L. is a medicinal and aromatic plant belonging to the Lamiaceae family. Originally native to Southern Europe and Asia, it is now cultivated worldwide for its nutritional and health benefits [1]. Its medicinal properties are primarily attributed to polyphenolic compounds, including phenolic acids and flavonoids [2]. Extensive research on *M. officinalis* leaf extracts has linked their phenolic compounds to various biological activities, such as anti-proliferative [3], anti-angiogenic [4], anti-viral [5], antioxidant [6], anxiolytic [2], anti-Alzheimer [7], anti-fungal [8], and anti-diabetic [9] effects. Although these polyphenols are widely recognized for their health-promoting properties, their practical application functional foods and therapeutics is often limited by inherent chemical instability and low oral bioavailability [10, 11]. Therefore, developing strategies to protect these compounds and enhance their bioavailability is essential.

Encapsulation is a highly effective approach for overcoming these limitations. Encapsulation facilitates targeted delivery to specific regions of the digestive tract by enclosing the active compound within a protective wall material [12]. Currently, spray drying is the most widely used encapsulation technology, due to its simplicity, rapid processing, and industrial scalability [13]. This technique involves atomizing a homogeneous mixture of core and wall materials into a drying chamber, where rapid solvent evaporation occurs. The size of the resulting samples ranges from micron- to nano-scale, depending on the spray dryer model [14]. However, conventional spray drying faces limitations when specific requirements, such as much smaller particle sizes, narrow size distributions, and highly controlled delivery are required. To address these challenges, nano spray drying technology has emerged as a superior alternative to produce encapsulated materials that offer improved dissolution rate, enhanced absorption, and greater bioavailability compared to conventional microcapsules [14]. For instance, Burki et al. utilized nano spray drying to produce smooth β-galactoside (2 – 4 µm) with a yield of (93.7%). Unlike conventional spray drying, which causes enzymatic activity loss, nano spray drying effectively preserved 92% of enzymatic activity after three weeks, demonstrating a notable advantage over conventional methods [15]. The successful formulation of encapsulated colloids via nano spray drying requires the precise control of key operational parameters, including inlet and outlet temperatures, atomization pressure, and airflow rate. These parameters directly influence the resulting particle size, morphological uniformity, and overall stability of encapsulated materials, thereby impacting encapsulation efficiency, structural integrity, and bioavailability active compounds [6, 9]. Furthermore, the choice of wall material is critical. Sodium alginate, a negatively charged, pH-sensitive biopolymer, exhibits excellent bioadhesive properties. It is highly effective at encapsulating both hydrophilic and lipophilic bioactive compounds, offering enhanced gastrointestinal protection andsuperior controlled release capabilities compared to other common biopolymers such as chitosan or gum Arabic [12, 16].

To the best of our knowledge, this is the first study to synergistically combine nano spray drying technology with a sodium alginate matrix to the encapsulation of *M. officinalis* phenolic compounds. The primary aim of this research was to develop and optimize the encapsulation system capable of enhancing the stability and controlled release of these bioactive compounds. The specific objectives included: screening the spray drying parameters to maximize encapsulation efficiency and achieve a target particle size enhancing encapsulation efficiency; characterizing the physicochemical properties, morphology, and thermal stability of the resulting particles; evaluating the preservation of antioxidant activity and the *in vitro* release kinetics under simulated gastrointestinal conditions; and elucidating the molecular-level interactions between rosmarinic acid, a key phenolic in *M. officinalis*, and the alginate matrix using spectroscopic analysis and molecular dynamics simulations. This multi-faceted approach aims to establish a platform for enhancing the bioavailability of *M. officinalis* phenolic compounds, thereby unlocking their full potential for future pharmaceutical and nutraceutical applications.

2. Materials and methods

2.1 Raw materials

Fresh *M. officinalis* leaves were harvested at the flowering stage from Soha Jissa Co. farm in Salmanshahr, Mazandaran, Iran. The plant material was air-dried and taxonomically characterized. A voucher specimen (No. 1/3650) was deposited at Soha Jissa Co. Sodium alginate and 2, 2-diphenyl-1-picrylhydrazyl (DPPH) were procured from Sigma-Aldrich (USA). Ethanol (99.5%) was obtained from Kimia Alcohol Zanjan (Zanjan, Iran). Potassium dihydrogen phosphate, sodium chloride, and hydrochloric acid (37%) were supplied by Merck (Darmstadt, Germany), and sodium hydroxide was obtained from BioChem (France). Milli-Q purified water was used throughout the analyses.

2.2 Plant material and extraction procedure

Four types of *M. officinalis* extracts were prepared using various solvents, including distilled water, 99.5% ethanol, and two hydroalcoholic mixtures (50% and 70% ethanol). For each solvent, a 10 g sample of dried and finely powdered plant material was macerated in 100 mL of the respective solvent. The extraction was carried out at room temperature for 24 h under continuous magnetic stirring at 300 rpm. Following maceration, the suspensions were filtered through filter paper to remove solid residues. The filtrates were then concentrated under reduced pressure using a rotary evaporator (Heidolph Hei-VAP Core) at a controlled temperature of 40 °C. The concentrated extracts were stored at 4 °C to maintain their stability and preserve their bioactive compounds for subsequent experimental use.

2.3 Phytochemical analysis

The polyphenolic composition of the extract was analyzed using an HPLC system (Alliance 2695 Separation Module, Waters, USA) equipped with a quaternary pump, in-line degasser, autosampler, and a Waters 2998 photodiode array (PDA) detector. Chromatographic separation was achieved using a SunFire C18 column (150 mm × 4.6 mm × 3.5 µm; Waters). Data acquisition and processing were performed using Empower 3 chromatography software (Waters, USA).

The mobile phase consisted of solvent A (water + 0.02% TFA) and solvent B (methanol + 0.02% TFA). The gradient elution program was as follows: 80% A and 20% B at 0 min; 20 – 30% B over 10 min; 30 – 40% B over 20 min; 40 – 80% B over 10 min; 80 – 100% B over 5 min; isocratic at 100% B for 5 min; and re-equilibration to 20% B for 5 min. The total run time was 55 min with a flow rate of 0.7 mL/min, an injection volume of 20 µL. Identification was performed at UV wavelengths from

https://doi.org/10.57647/pibm.2026.152604

200 to 400 nm with 1.2 nm resolution. For all HPLC analyses, samples were dissolved in ethanol (1 mg/mL) and analyzed in triplicate.

Quantitative analysis of major polyphenols such as caffeic acid, rosmarinic acid, rutin, catechin, and chicoric acid was performed by comparing retention times and UV spectra with analytical-grade external standards. To ensure accuracy, calibration curves were generated for each compound across of 0.00312 to 0.1 mg/mL, all demonstrating strong linearity correlation coefficients ($R^2 \geq 0.99$). The calibration equations at optimal detection wavelengths were as follows: caffeic acid ($y = 146733.0791x - 245327.8813$ at 324 nm), rutin ($y = 24590.8351x - 70251.4886$ at 254 nm), rosmarinic acid ($y = 91131.594x - 707594.6841$ at 330 nm), catechin ($y = 26808x - 110855$ at 279 nm), and chicoric acid ($y = 6201.9x - 49571$ at 330 nm).

2.4 Spray drying parameters for efficient encapsulation of extracts

In this study, ten formulations (F1–F10) were prepared to investigate the effects of critical spray drying parameters on encapsulation efficiency, particle size distribution, and antioxidant retention of *M. officinalis* extract within sodium alginate matrix. While the core-to-wall ratio and total solid concentration were maintained at constant values for all formulations, the operating parameters including airflow rate, inlet temperature, and atomization pressure were systematically varied to identify the most favorable conditions for the encapsulation process.

For the preparation of the feed solutions, sodium alginate (500 mg) was dissolved in 50 mL of distilled water and stirred overnight at 700 rpm to ensure full polymer hydration. Separately, an aqueous solution of the extract (100 mg in 50 mL distilled water) was prepared. After complete dissolution, the extract solution was combined with the hydrated polymer. This final mixture was homogenized by stirring at 500 rpm for two hours.

Encapsulation was carried out using an NSD25 nano spray dryer (Tadbir Tarah Co., Mashhad, Iran). The system featured a 0.2 mm two-fluid nozzle, optimized for the production of uniform particles and the thermal protection of labile bioactive compounds. The ten formulations were subjected to different processing conditions, comprising airflow rates (50 and 100 cm^3/s), inlet temperatures (100 – 165 °C), and atomization pressures (4 and 5 bar), as detailed in Table 1.

2.5 Encapsulated particle analysis

2.5.1 Determination of PY, EE, and LC

Powder yield (PY) was determined as the percentage of the dried product recovered relative to the total solid mass in the initial feed solution, calculated using the following equation (1) [17]:

$$PY = \frac{(W_2 - W_1) - X_{wb}(W_2 - W_1)}{MVTS} \times 100 \quad (1)$$

where PY is the powder yield (%), X_{wb} is the moisture content of the sample on a wet basis, M_V is the volume of feed solution (L), T_S is the total solids content (g dry matter/L), W_1 is the weight of the container before drying (g), and W_2 is the weight of the container after drying (g). Encapsulation efficiency (EE) represents the percentage of phenolic compounds successfully entrapped within the encapsulated materials. This parameter was calculated using a modified method adapted from [18] and calculated according to the equation (2):

$$EE(\%) = \frac{\text{Mass of loaded phenolic content}}{\text{Mass of initial phenolic conten}} \times 100 \quad (2)$$

To determine the total phenolic content, 10 mg of the encapsulated colloids were dispersed in a solvent mixture composed of ethanol, acetic acid, and water in a ratio of 50:8:42. The mixture was vortexed for 1 min, ultrasonicated at 80 kHz for 20 min, and subsequently centrifuged at 9500 rpm for 10 min. The resulting supernatant was filtered through a 0.45 µm membrane filter [19]. A standard calibration curve with a determination coefficient $R^2 = 1$ was prepared using gallic acid solutions at concentrations of 3.125, 6.25, 12.5, 25, and 50 ppm in the ethanol-acetic acid-water mixture.

The surface phenolic content (SPC) was determined by dissolving 10 mg of encapsulated materials in 2 mL of an ethanol:methanol mixture (1:1). The dispersion was vortexed for 1 min and filtred through a 0.45 µm membrane filter [19]. A corresponding standard calibration curve ($R^2 = 0.9978$) was prepared using gallic

Table 1. Spray drying formulations and process conditions used for encapsulation optimization.

Code	IT (°C)	OT (°C)	AP (bar)	AFR (cm^3/s)	TFA (mg/mL)
F1	100	51.6	4	50	600
F2	100	54.6	4	100	600
F3	100	48.1	5	50	600
F4	100	50.5	5	100	600
F5	115	58.5	4	50	600
F6	115	58.5	4	100	600
F7	125	67	4	50	600
F8	125	60.6	4	100	600
F9	145	63.2	4	100	600
F10	165	63.7	4	100	600

IT: Inlet temperature; OT, Outlet temperature; AP, Atomizer Pressure; AFR, Airflow rate; TFA, Total Feed Amount.

https://doi.org/10.57647/pibm.2026.152604

acid solutions across the same concentration range in the 50:50 ethanol-methanol solvent mixture. Absorbance values of the filtered supernatants were measured using a UV-Vis spectrophotometer (UV-250 1PC, Shimadzu) over a wavelength range of from 200 to 400 nm.

The loading capacity (LC) was defined as the percentage of the mass of the encapsulated phenolic compounds relative to the total mass of the sample [18]. LC was calculated according to the formula (3):

$$\text{LC}(\%) = \frac{\text{Mass of loaded phenolic content}}{\text{Mass of sample}} \times 100 \quad (3)$$

2.5.2 Particle size distribution and morphological analysis

The particle size distribution of the spray-dried particles was analyzed by dynamic light scattering (DLS) using a Nanophox instrument (Sympatec GmbH, Clausthal, Germany) to determine their hydrodynamic diameters. The morphology of the encapsulated materials was examined by field emission scanning electron microscopy (FESEM, model MIRA2, TESCAN, Czech Republic). Prior to imaging, the samples were sputter-coated with a 10 nm gold layer to enhance conductivity and image quality. The obtained FESEM images were analyzed using image software to generate size distribution plots, enabling a comprehensive evaluation of particle uniformity and dispersion.

2.5.3 Moisture content

The moisture content of the particles was determined in accordance with the United States Pharmacopeia (USP) guidelines for analyzing moisture in pharmaceutical products. Briefly, 20 mg of sample was accurately weighed into a glass container and heated in an oven at 105 °C for 5 h. The weight of each sample was meticulously recorded before and after the drying process. The moisture content was then calculated based on the weight difference observed during the drying phase [20].

2.5.4 FTIR spectroscopy and thermal analysis

Molecular interactions between the encapsulated phenolic compounds and the sodium alginate matrix were investigated by Fourier-transform infrared (FTIR) spectroscopy and differential scanning calorimetry (DSC) analyses. FTIR spectra were recorded using a Tensor 27 spectrometer (Bruker, Germany). Each sample was mixed with potassium bromide at a 1:100 (w/w) ratio and compressed into transparent pellets using a hydraulic press. Spectral data were collected over a wavenumber range of 400 – 4000 cm^{-1} [21].

DSC analysis was performed using a thermal analyzer (model TGA-50, Shimadzu, Japan) to investigate the thermal properties, stability, and potential phase transitions of the encapsulated colloids. Approximately 3.5 mg of each sample was hermetically sealed in an aluminum pan. Each sample was placed in the instrument and equilibrated at 0 °C for 5 min to ensure thermal equilibrium with the reference. Subsequently, the measurements were recorded as the samples were heated from 0 °C to 600 °C at a constant rate of 10 °C/min under a continuous nitrogen flow of 30 mL/min [22].

2.5.5 Antioxidant activity

The antioxidant activity of both the encapsulated and free phenolic compounds was determined using the DPPH radical scavenging assay, following the method described by Markus et al., with minor modifications [23]. Samples at various concentrations were prepared in an ethanol: methanol mixture (1:1) and mixed with 0.2 mm DPPH solution. After vortexing, the mixtures were incubated in the dark at 25 °C for 30 min. The absorbance was recorded at 517 nm using a microplate reader. IC_{50} values were calculated by non-linear regression of the inhibition percentage versus the sample concentration. Furthermore, to establish a normalized baseline for comparing the encapsulated formulations with the free extract, an estimated IC_{50} (EC) was theoretically calculated. This EC value was adjusted proportionally based on the specific EE of each encapsulated formulation. All assays were performed in quadruplicate, and results are expressed as mean ± standard deviation (SD).

2.5.6 Release profiles

The release profile of *M. officinalis* extract from alginate encapsulated materials was evaluated in simulated gastric fluid (SGF) and simulated intestinal fluid (SIF), as described by Saadatidizaji et al., with slight modifications [24]. The SGF was prepared by dissolving 5 g of NaCl in 125 mL of distilled water, diluting the volume to 250 mL, and setting the pH to 1.2 using 37% HCl. To evaluate gastric release, 3 mg of the encapsulated samples were dispersed in 25 mL of SGF and incubated at 37 °C under continuous stirring for 2 h. For the intestinal release study, a phosphate buffer solution (pH 6.8) was used to simulate intestinal conditions. Similarly, 3 mg of encapsulated materials were dispersed in 25 mL of the SIF buffer and incubated at 37 °C for 4 h. The mass of the polyphenol compounds released into the medium was determined using the procedure previously described in Section 2.5.1. The percentage of the extract released was calculated using the following formula:

$$\text{Released extract}(\%) = \frac{M_c}{M_e} \times 100 \quad (4)$$

where M_c represents the mass of the released polyphenols, and M_e is the total mass of encapsulated polyphenols.

2.6 Swelling index

In this study, the swelling behavior of the optimized formulation (F6) was evaluated in simulated gastric fluid (SGF, pH 1.2). Briefly, 200 mg of the sample was accurately weighed (W_0) and dispersed in 50 mL of SGF. The suspension was incubated in a shaker (Heidolph, Germany) at 37 ± 0.5 °C with constant agitation at 60 rpm for 2 h. After incubation, the swollen particles were collected, gently blotted with filter paper to remove excess surface liquid, and weighed again (W_f) [25, 26].

The swelling index was calculated using the following equation:

$$\text{Swelling index} = \frac{W_f - W_0}{W_0} \times 100 \quad (5)$$

where W_0 is the initial weight of the dry sample and W_f is the weight of the swollen sample after incubation, and the results were expressed as mean ± SD.

2.7 Storage stability

The storage stability of the encapsulated samples was evaluated by storing 2 g of each formulation in airtight plastic containers at 37 °C for two months. Following the storage period, 10 mg of each sample was analyzed for its rosmarinic acid content, a key marker compound in the 70% hydroalcoholic extract of *M. officinalis*, using HPLC-PDA. The unencapsulated extract was also analyzed as a control to assess the stability of rosmarinic acid in its free form. The percentage of the retained rosmarinic acid was quantified to determine the storage stability of the encapsulated extract and to estimate the potential shelf life of the product.

2.8 Colloidal stability analysis

Formulation F6 was selected as a representative sample for stability evaluation. The physical stability of the encapsulated materials was assessed by measuring the hydrodynamic diameter and zeta potential using a Zetasizer Nano ZS instrument (Malvern, UK). Analyses were performed at 10-day intervals over a 30-day period following production. These measurements were used to monitor changes in the particle size distribution and surface charge, providing critical insights into the colloidal stability of the formulation over time.

2.9 Molecular docking and dynamics simulations

Molecular docking was employed to evaluate the binding interactions between rosmarinic acid and the sodium alginate polymer matrix. The computational study was conducted following five key steps: polymer preparation, ligand preparation, receptor grid generation, ligand docking, and analysis of results. Alginate polymer structures were built using the Polymer Builder module (version 14.0) in Maestro 2024 (Schrödinger, LLC). For monomer units unavailable within the software library, chemical structures were retrieved from the PubChem database and processed accordingly. The polymer structures were optimized with the OPLS4 force field and energy-minimized using the truncated Newton conjugate gradient method in MacroModel, employing 2500 iterations and an energy convergence threshold of 0.05 kcal/mol. Linear alginate polymers were generated using default initiator and terminator settings. Ligands were prepared with the LigPrep module, converting 2D molecular structures into energy-minimized 3D conformations using the OPLS4 force field. Grid generation for docking was performed in the Glide module, with the active site bounding box centered at coordinates (X: −0.95, Y: 1.4, Z: 2.11) and sized to encompass the entire ligand-polymer interaction interface.

To assess the stability of the rosmarinic acid–alginate complex under simulated physiological conditions, molecular dynamics (MD) simulations were conducted in the Desmond module. Two distinct simulations were performed: a 10 ns run with a 3 Å buffer to examine local atomic-scale interactions, and a 30 ns run with a 10 Å buffer to evaluate broader structural dynamics. These simulations provided insights into hydrogen bonding, van der Waals interactions, and conformational flexibility, confirming the structural stability and adaptability of the complex in a solvated environment.

2.10 Statistical analysis

The experimental data were subjected to one-way analysis of variance (ANOVA), followed by Tukey's honestly significant difference (HSD) post hoc test to determine statistically significant differences among the experimental groups. Statistical analyses were performed using GraphPad Prism software (version 10.3.1; GraphPad Software, San Diego, CA, USA). A significance level of $p < 0.05$ was considered statistically significant for all comparisons. Each experiment was conducted in triplicate to ensure reproducibility.

3. Results and discussion

3.1 HPLC-PDA phenolic profiling of *M. officinalis* extracts

The rosmarinic acid content in various *M. officinalis* extracts was quantified using HPLC-PDA. The 70% hydroalcoholic extract exhibited the highest rosmarinic acid content at 8.97 mg/g of dry extract, with an extraction yield of 40.00% (Fig. 1 (a)). In comparison, the 50% hydroalcoholic extract contained 7.06 mg/g (yield: 38.2%) (Fig. 1 (b)), followed by the alcoholic extract (99.5%) with 4.27 mg/g (yield: 33.49%) (Fig. 1 (c)). In contrast, the crude aqueous extract showed only trace amounts of rosmarinic acid (Fig. 1 (d)). These results identified the 70% hydroalcoholic extract as the most efficient formulation regarding phenolic content, particularly rosmarinic acid, justifying its selection for subsequent encapsulation studies.

Further phenolic profiling of the 70% hydroalcoholic extract of *M. officinalis* via HPLC-PDA enabled the quantification of key bioactive constituents. The analysis revealed the presence of catechin (0.16 ± 0.05 mg/g), caffeic acid (0.12 ± 0.04 mg/g), chicoric acid (2.41 ± 0.06 mg/g), rutin (0.47 ± 0.01 mg/g), and rosmarinic acid (8.97 ± 0.05 mg/g) (Table 2). These phenolic compounds are highly recognized for their potent antioxidant, anti-inflammatory, and therapeutic properties, supporting the selection of this extract for functional food and pharmaceutical applications.

The superior extraction efficiency observed with the 70% hydroalcoholic solvent system can be attributed to its intermediate polarity, which enhances the solubilization of both hydrophilic and moderately lipophilic phenolic compounds compared to pure ethanol or water alone. Notably, the rosmarinic acid content obtained from the 70% hydroalcoholic extract in this study (8.97

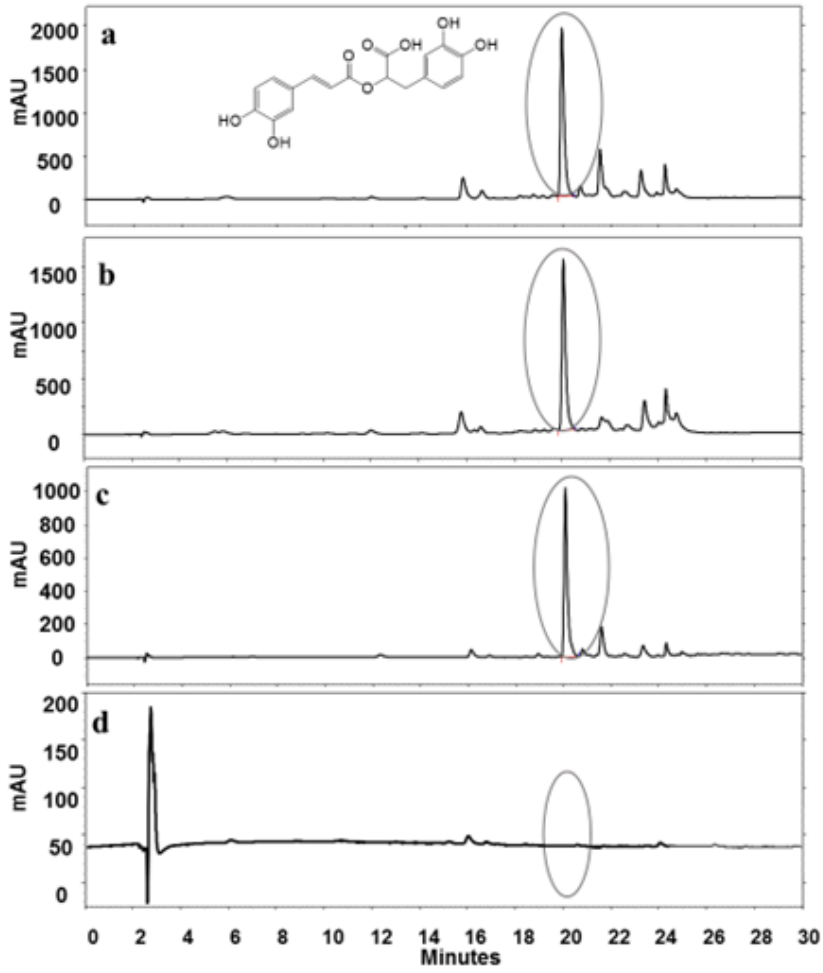

Figure 1. Chromatographic profiles of *M. officinalis* extracts: (a) Hydroalcoholic extract (70%), (b) Hydroalcoholic extract (50%), (c) Alcoholic extract (99.5%), (d) Crude aqueous extract, as determined by HPLC-PDA analysis.

± 0.05 mg/g) exceeded previously reported values of 6.91 ± 0.78 mg/g [27], 3.50 ± 0.002 mg/g [28], and 8.63 mg/g [27], highlighting the efficacy of the utilized extraction method. These results align with the literature, which indicates that binary solvent mixtures, such as methanol–water or ethanol-water, generally yield higher phenolic contents than aqueous systems alone [29]. Consequently, the 70% hydroalcoholic extract was selected as the optimal formulation for encapsulation owing to its enriched phenolic profile and high extraction yield.

3.2 Morphology and size distribution of encapsulated materials

FESEM micrographs (Fig. 2) showed that the inlet air temperature significantly affected the surface morphology and apparent geometric size of sodium alginate encapsulated colloids. At the lowest temperature evaluated (F2: 100 °C; 4 bar; 100 cm^3/s), the encapsulated materials were predominantly spherical, uniform, and relatively small, exhibiting smooth surfaces with minimal aggregation or adhesion. These characteristics are consistent with mild drying conditions that facilitate gradual water removal, the formation of a mechanically robust polymeric shell, and limited surface wrinkling, thereby preserving the structural integrity of the materials [30]. Increasing the inlet temperature to 115 °C (F6) largely maintained the spherical morphology but induced more pronounced surface wrinkles and shallow indentations, indicating a higher drying rate and greater surface stress on the polymer shell. At 125 °C (F8), the materials exhibited a significant increase in wrinkling, deeper indentations, and distinct folding. This morphol-

Table 2. Polyphenolic composition determined by HPLC-PDA, expressed in mg/g of extract (mg/g E).

Compound name	Rt (min)	Content (mg/g of dry extracts)
Catechin	11.787	0.16 ± 0.05
Caffeic acid	17.077	0.12 ± 0.04
Chicoric acid	25.262	2.41 ± 0.06
Rutin	26.362	0.47 ± 0.01
Rosmarinic acid	28.290	8.97 ± 0.05

https://doi.org/10.57647/pibm.2026.152604

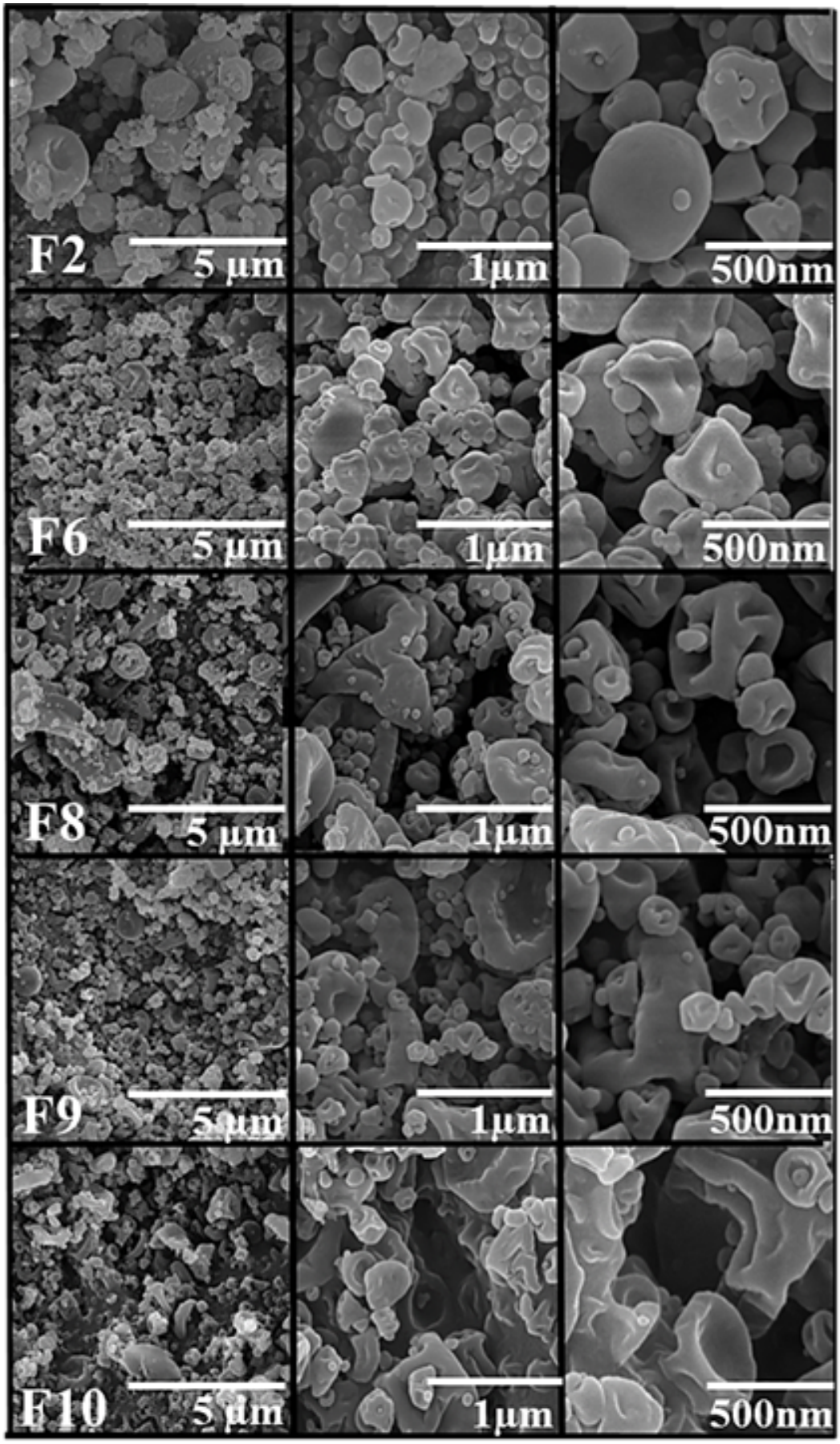

Figure 2. Field Emission Scanning Electron Microscopy (FESEM) images, with corresponding scale bars of 5 µm, 1 µm, and 500 nm, of sodium alginate encapsulated materials produced by spray drying at inlet air temperatures of 100 °C (F2), 115 °C (F6), 125 °C (F8), 145 °C (F9), and 165 °C (F10).

https://doi.org/10.57647/pibm.2026.152604

ogy suggests very rapid shell formation combined with a decrease in feed viscosity, conditions that favor the development of internal cavities and local collapse during moisture evaporation [31].

Further elevation of the inlet temperature to 145 °C (F9) yielded severely wrinkled particles with highly indented and irregular surfaces. The highest temperature assessed (F10, 165 °C) produced the most deformed particles, characterized by extensive shell deformation, deep cavities, and pronounced surface roughness. Such extreme drying conditions maximize thermal and mechanical stresses on the biopolymer matrix and, consistent with previous reports, are typically associated with reduced encapsulation efficiency due to structural damage of the carrier matrix.

Consistent with these morphological alterations, the FESEM-based mean diameters increased substantially with elevated temperature. The average apparent diameters at 100, 115, 125, 145 and 165 °C were 584.4 ± 12.3, 620 ± 17.43, 750.2 ± 4.00, 800.5 ± 4.1, and 997.84 ± 23.1 nm, respectively. Thus, higher inlet air temperatures promoted not only the formation of larger particles but also the development of more pronounced internal voids and cavitated structures [32]. This behavior can be attributed to the accelerated drying process, which rapidly generates a rigid outer layer while internal vapor pressure simultaneously rises. The trapped vapor drives particle swelling and the formation of hollow or partially hollow structures, which manifest as wrinkled, shelled materials with reduced density in FESEM images. Overall, a direct correlation was established between increasing drying air temperature, particle size growth, and the intensity of cavitation and wrinkling, which aligns with previous studies on spray dried biopolymer systems [33].

DLS provided complementary information on the hydrodynamic particle size (PS) and polydispersity index (PDI) of the redispersed encapsulated material suspensions. Across the evaluated formulations, PS ranged from approximately 714 to 1445 nm, with PDI values between 0.2 to 0.6, indicating medium to relatively broad size distributions. Samples produced at mild to moderate temperatures (PS ≈ 714 – 862 nm, PDI 0.2 – 0.5) displayed smaller hydrodynamic diameters and acceptable polydispersity, which is consistent with the more compact and less cavitated structures observed by FESEM. In contrast, formulations exposed to higher inlet temperatures and more intense drying conditions showed the highest hydrodynamic sizes (PS ≈ 1439 – 1445 nm). However, they maintained PDI values around 0.3 – 0.4, suggesting overall particle expansion and partial agglomeration without resulting in an extremely heterogeneous population. A comparison of the FESEM and DLS data highlights the complementary nature of these techniques. FESEM visualizes the geometric size and surface topology of the dried particles, clearly revealing cavity formation and shell deformation. In contrast, DLS measures the hydrodynamic diameter of the particles dispersed in an aqueous medium, a parameter sensitive to solvation layers, swelling, and reversible aggregation. Formulations processed at high temperatures, which appeared wrinkled and hollow in FESEM, exhibited markedly increased hydrodynamic diameters in DLS analysis. This reflects both the larger primary particle size and the propensity of rough, low density particles to form loose clusters in suspension. Conversely, the smoother and more compact particles obtained at lower temperatures redispersed more efficiently, yielding smaller PS values and, in certain cases, lower PDI.

Taken together, the combined FESEM and DLS analyses indicate that controlling the inlet air temperature within an intermediate range is critical for obtaining encapsulated colloids with favorable morphology, moderate size, and an acceptable size distribution. Excessively low temperatures may compromise drying efficiency, whereas excessively high temperatures promote extensive cavitation, severe wrinkling, and particle expansion, ultimately leading to larger hydrodynamic sizes and potentially reducing encapsulation performance. Therefore, the optimization of spray drying temperature is imperative to balance morphological integrity with size control, ensuring the production of stable sodium alginate-encapsulated materials suitable for biological and pharmaceutical applications.

3.3 Effects of spray drying parameters on production yield, encapsulation efficiency, and loading capacity

Increasing the inlet air temperature of the spray dryer significantly enhanced the production yield of spray-dried encapsulated colloids (Table 1 and 3), which is consistent with previous reports [34]. The yield was lowest at 100 °C (33.39 ± 0.18%), rising progressively to 37.55 ± 0.15% at 115 °C, 45.00 ± 0.16% at 125 °C, 49.36 ± 0.02% at 145 °C, and 50.00 ± 0.11% at 165 °C. This improvement is attributed to enhanced heat transfer at higher temperatures, which facilitates rapid moisture evaporation and reduces the adherence of carrier materials to the dryer chamber walls, thereby improving production efficiency [35].

The effect of airflow rate on production yield varied depending on the inlet temperature. At 100 °C, increasing the airflow rate from 50 to 100 cm^3/s decreased the yield, while at higher temperatures (115 °C and 125 °C), an equivalent increase in flow rate (F5→F6, F7→F8) improved efficiency. These results suggest that at lower inlet temperatures, airflow rate has a more pronounced impact on efficiency than the temperature itself. Conversely, at elevated temperatures, the inlet air temperature dominates the efficiency outcome. Furthermore, increasing the inlet air temperature reduced the SPC of the encapsulated materials (Table 3). This reduction is likely due to the accelerated drying process, which rapidly fortifies the polymer membrane and hinders the diffusion of core materials to the surface, in agreement with previous findings [27, 28].

The size of the encapsulated materials showed no statistically significant effect on encapsulation efficiency, as both smaller and larger air-dried colloids demonstrated

Table 3. The physicochemical properties, including product yield (PY), encapsulation efficiency (EE), loading capacity (LC), particle size (PS), polydispersity index (PDI), moisture content (MC), and surface phenolic content (SPC).

code	PY (%)	EE (%)	SPC (mg)	LC	MC (%)	PS (nm)	PDI
F1	52.12 ± 0.07^{a}	84.68 ± 4.99^{bd}	0.17 ± 0.02^{bc}	9.38 ± 4.49^{ac}	5.0 ± 0.20^{c}	751.6 ± 23.6^{ce}	0.20 ± 0.01^{bc}
F2	33.39 ± 0.18^{e}	78.28 ± 0.73^{d}	0.43 ± 0.02^{a}	15.46 ± 0.1^{a}	5.0 ± 0.20^{c}	714.2 ± 10.3^{e}	0.50 ± 0.01^{ab}
F3	22.87 ± 0.46^{g}	80.26 ± 2.79^{cd}	0.15 ± 0.02^{bc}	6.10 ± 0.5^{c}	15 ± 0.10^{a}	749.5 ± 29.2^{ce}	0.60 ± 0.01^{a}
F4	16.5 ± 0.6^{h}	90.91 ± 1.84^{ab}	0.15 ± 0.01^{bc}	14.96 ± 4.41^{a}	10 ± 0.00^{b}	733.0 ± 18.2^{de}	0.50 ± 0.09^{a}
F5	31.19 ± 0.07^{f}	91.36 ± 0.63^{a}	0.07 ± 0.004^{d}	7.39 ± 0.65^{bc}	5.0 ± 0.20^{c}	1439.5 ± 36.6^{a}	0.40 ± 0.0005^{ac}
F6	37.55 ± 0.15^{d}	88.65 ± 0.57^{ab}	0.21 ± 0.04^{b}	16.39 ± 3.12	5.0 ± 0.20^{c}	862.8 ± 11.4^{ce}	0.30 ± 0.05^{ac}
F7	30.91 ± 0.87^{f}	87.04 ± 4.25^{abc}	0.14 ± 0.06^{bd}	9.39 ± 0.35^{ac}	15 ± 0.40^{a}	1445 ± 14^{a}	0.30 ± 0.02^{ac}
F8	45.00 ± 0.16^{c}	87.42 ± 1.57^{abc}	0.2 ± 0.01^{bc}	13.90 ± 2.74^{ab}	10 ± 0.10^{b}	938.00 ± 5.7^{bcd}	0.30 ± 0.01^{ac}
F9	49.36 ± 0.02^{b}	89.22 ± 0.52^{ab}	0.18 ± 0.01^{bc}	14.86 ± 0.20^{a}	15 ± 0.20^{a}	959.00 ± 8.27^{bc}	0.20 ± 0.03^{c}
F10	50.00 ± 0.11^{b}	84.34 ± 2.37^{ad}	0.13 ± 0.02^{cd}	7.00 ± 0.41^{bc}	0.00 ± 0.00^{d}	1111.50 ± 16^{b}	0.30 ± 0.04^{ac}

Different superscript letters in same column indicate statistically significant differences by the Tukey's HSD test ($p < 0.05$).

comparable entrapment values. This aligns with existing literature, which frequently reports inconclusive correlations between carrier size and encapsulation efficiency [29, 30]. Although higher inlet temperatures were theoretically expected to enhance encapsulation efficiency by rapidly forming a semi-permeable membrane around droplets, excessively high temperatures adversely affected the final dried product. Specifically, thermal degradation, structural ballooning induced by internal vapor pressure, and the formation of surface defects increased the loss of active material, ultimately reducing the encapsulation efficiency [31, 32, 33, 34, 35, 36]. Maintaining a constant temperature of 100 °C while raising the atomization pressure to 5 bar (T: 100, P: 5, B: 100) substantially enhanced encapsulation efficiency to 90.91 ± 1.84% (Table 1 and 3). As previously established by King (1995), higher atomization pressure improves the dispersion and mobility of droplets, which in turn increases hot air entrainment. This accelerates both the drying process and the formation of the protective polymeric film, thereby enhancing the retention of active materials [37]. Smaller particles with an average diameter of 620 nm (T: 115 °C, P: 4 bar, B: 100; F6) showed the highest LC at 16.39 ± 3.12% (Table 3). In contrast, larger encapsulated materials exhibited a reduced phenolic loading. This observation is consistent with literature indicating that medium-to-small-sized carrier systems often demonstrate superior retention of active compounds, whereas excessively large structures are prone to diminished encapsulation efficiencies and lower core loadings [38, 39].

3.4 Moisture content analysis

The moisture contents of the spray-dried formulations are shown in Table 3. Maintaining a residual moisture level at or below 5% is generally considered optimal for inhibiting microbial proliferation and lipid oxidation, thereby ensuring the long-term storage stability of powdered products [36]. Formulations F1, F2, F5, F6, and F10 showed moisture contents proximate to this critical threshold, indicating their suitability for prolonged storage. Conversely, higher moisture contents (10 – 15%) significantly increase the susceptibility of the product to microbial contamination and chemical degradative reactions, such as hydrolysis and oxidation, which inevitably lead to deterioration in quality over storage time. Furthermore, moisture content is a critical determinant of powder flowability, caking tendency, and dispersibility; specifically, powders with lower moisture profiles show superior handling characteristics and reduced propensity for agglomeration [40]. The final moisture content of the spray-dried product is profoundly affected by the operational drying parameters, particularly the inlet air temperature, atomization pressure, and airflow rate. The precise optimization of these parameters facilitates efficient moisture removal without inducing thermal cracking or surface collapse of the encapsulated colloids [21]. In this study, formulations presenting lower moisture contents showed improved encapsulation efficiencies and production yields (Table 3), indicating that controlled drying dynamics preserve the structural integrity of the polymer shell and enhance the stability of the encapsulated phenolic compounds.

3.5 Antioxidant capacity of the encapsulated materials

Table 4 summarizes the total antioxidant capacity of the spray-dried formulations (F1-F10), evaluated based on TPC and DPPH radical scavenging activity (IC_{50}). Among all evaluated samples, formulations F5 and F6 showed the highest antioxidant potential, with IC_{50} values comparable to that of the gallic acid reference. This indicates the efficient thermal preservation and high bioavailability of the encapsulated phenolic compounds. In contrast, formulations characterized by lower phenolic contents displayed significantly higher IC_{50} values, suggesting a reduced radical scavenging efficiency. Furthermore, the theoretically calculated IC_{50} values followed a pattern highly similar to the experimental IC_{50} results, confirming the internal consistency among the retained phenolic content, encapsulation efficiency, and resultant antioxidant activity.

https://doi.org/10.57647/pibm.2026.152604

Table 4. Total antioxidant capacity of the formulations, including total phenolic content (TPC), experimental DPPH radical scavenging activity (IC_{50} (µg/mL), and expected calculated (EC) IC_{50}.

code	TPC	IC_{50} (µg/mL)	EC IC_{50}
F1	1.11 ± 0.49^{bd}	17157.14 ± 12.5^{b}	14454.93 ± 177.14^{a}
F2	1.98 ± 0.01^{a}	889.90 ± 4.3^{h}	695.74 ± 13.91^{h}
F3	0.76 ± 0.03^{d}	17609.90 ± 0.2^{a}	14205.90 ± 457.78^{b}
F4	1.65 ± 0.49^{abc}	1296.60 ± 14.7^{f}	1175.89 ± 50.44^{f}
F5	0.81 ± 0.07^{d}	134.65 ± 15.72^{i}	123.07 ± 17.40^{i}
F6	1.85 ± 0.29^{ab}	104.88 ± 4.11^{ij}	92.99 ± 5.47^{j}
F7	1.08 ± 0.09^{cd}	2079.90 ± 15.72^{d}	1813.01 ± 86.21^{d}
F8	1.59 ± 0.26^{abc}	1165.70 ± 13.90^{g}	1021.69 ± 49.70^{g}
F9	1.67 ± 0.02^{abc}	1393.90 ± 10.9^{e}	1242.81 ± 48.04^{e}
F10	0.83 ± 0.07^{d}	2776.60 ± 22.2^{c}	2333.21 ± 27.28^{c}
Gallic acid	-	93.80 ± 1.3^{j}	-

TPC, total phenolic content; EC IC_{50}, expected calculated IC_{50}, (the theoretically estimated IC_{50} value, calculated by assuming that an equivalent concentration of the extract was subjected to DPPH analysis (based on EE% presented in Table 4), establishing a normalized baseline for comparison. Different letters in same column indicate statistically significant differences by the Tukey's HSD test ($p < 0.05$).

3.6 FTIR analysis

Formulation F6, identified as the most favorable sample (PS ≈ 620 nm, EE = 88.65 ± 0.57%, LC = 16.39 ± 3.12%), was selected for detailed FTIR analysis to confirm molecular interactions and encapsulation stability. The FTIR spectrum of pure sodium alginate exhibited characteristic bands, including a broad O-H stretching vibration at 3405 cm^{-1} (hydrogen bonding), saccharide ring vibrations at 1078 and 1155 cm^{-1}, and carboxyl group (-COOH) symmetric/asymmetric stretching at 1452 and 1650 cm^{-1}, respectively [21]. The pure *M. officinalis* extract displayed a broad O-H stretching region (3155 – 3766 cm^{-1}), an aliphatic C-H stretch at 2927 cm^{-1}, and an intense C=C/C=O stretch at ~1606 cm^{-1}, which is indicative of flavonoid conjugation. In the spectrum of F6 encapsulated formulation, notable spectral shifts were observed. The O-H band shifted to 3421 cm^{-1} and exhibited reduced intensity, suggesting the formation of new hydrogen bonds between the phenolic hydroxyl groups of the extract and the carboxyl groups of the alginate matrix. Furthermore, the C=O stretch of extract flavonoids shifted from 1606 to 1612 cm^{-1}, accompanied by the broadening of the saccharide peaks at 1078 – 1155 cm^{-1}. Collectively, these spectral variations confirm the successful physical incorporation of the plant polyphenols into the alginate matrix without inducing chemical degradation of the active compounds (Fig. 3).

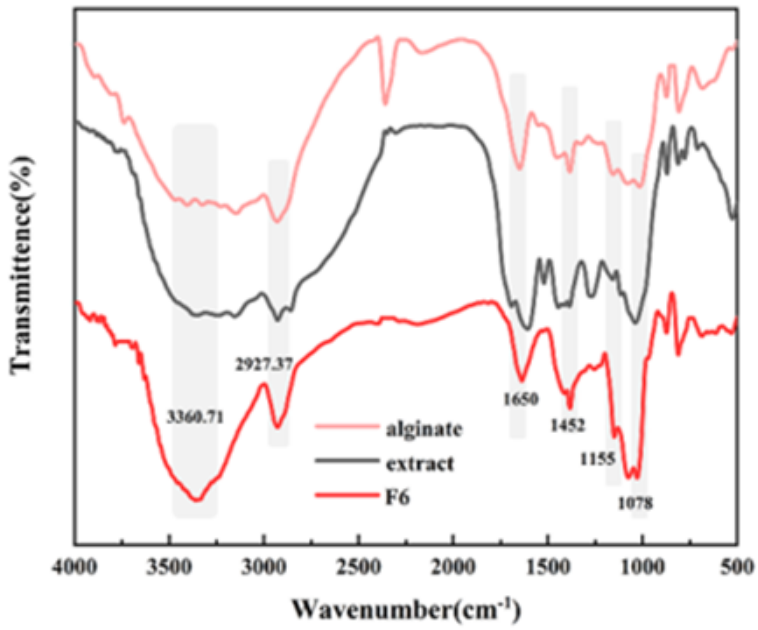

Figure 3. FTIR spectra of various samples, including pure sodium alginate, pure *M. officinalis* extract, and encapsulated formulation F6. The spectra reveal characteristic functional groups and specific molecular interactions, demonstrating the successful encapsulation of the extract within the alginate matrix. This is evidenced by distinct shifts and variations in peak intensities in the encapsulated formulations compared to the spectra of the pure components.

https://doi.org/10.57647/pibm.2026.152604

3.7 DSC thermophysical properties

DSC was employed to investigate the thermal behavior and stability of pure sodium alginate, free *M. officinalis* extract, and the selected encapsulated formulation (F6) (Fig. 4). The thermogram of sodium alginate displayed a broad low-temperature endothermic region starting around 34 – 43 °C, reaching a maximum at approximately 80 – 90 °C, and ending near 114 – 134 °C. This region is generally attributed to the loss of bound water and physical relaxation of the polysaccharide network rather than chemical degradation, and this extensive dehydration process effectively masks the detection of a distinct glass transition temperature (T_g) [41]. At higher temperatures, alginate exhibited two major decomposition stages: a first process with an onset in the 330 – 355 °C range and a peak around 370 – 385 °C, followed by a second, more intense endothermic event between 488 and 518 °C. These events correspond to backbone scission and decarboxylation of uronic acid residues, ultimately leading to char formation [42]. The free *M. officinalis* extract showed a distinct low- to mid-temperature endothermic event with an onset around 40 – 45 °C, a peak near 80 – 100 °C, and an endset in the 110 – 120 °C region, which can be ascribed to evaporation of residual moisture and melting or softening of low-melting phenolic constituents. At higher temperatures, sharp exothermic peaks with onsets around 330 – 340 °C and 420 – 425 °C indicated rapid thermal decomposition and oxidation of low-molecular-weight polyphenols. This confirms the limited intrinsic thermal stability of the non-encapsulated extract and its susceptibility to abrupt degradation within a relatively narrow temperature range [43].

In contrast, the DSC thermogram of the formulation F6 revealed a broad low-temperature endotherm spanning approximately 20 – 170 °C. While this lower-temperature transition primarily reflects residual moisture removal and the plasticization of the polymer network the actual evidence of enhanced thermal stability lies in the higher-temperature thermal events with an overall enthalpy intermediate between that of pure alginate and the free extract. Notably, the distinct, sharp melting and exothermic decomposition peaks characteristic of the free extract were completely absent in the of F6 thermogram. Instead, the main decomposition profile of F6 was shifted upward, closely mirroring the primary degradation region of the alginate matrix. The disappearance of the specific thermal transitions of the extract indicates that the phenolic constituents were successfully entrapped and molecularly dispersed in an amorphous state within the alginate matrix, rather than existing as crystalline domains. This physical state transition, driven by strong intermolecular interactions such as hydrogen bonding and electrostatic association between alginate carboxylate groups and phenolic or carboxylic groups of the extract, acts as a barrier against heat [44].

Taken together, these results demonstrate that encapsulation within the alginate network markedly modifies the physical state of *M. officinalis* polyphenols and shields them from thermal stress. The upward shift of the main degradation temperature, the disappearance of discrete extract-specific transitions, and the transition to a more gradual decomposition profile collectively show that the biopolymer matrix acts as a thermal shield, delaying the onset of thermal degradation and preventing abrupt exothermic decomposition of the polyphenols. This improved thermal stability is highly advantageous for bioactive delivery systems that must withstand thermal

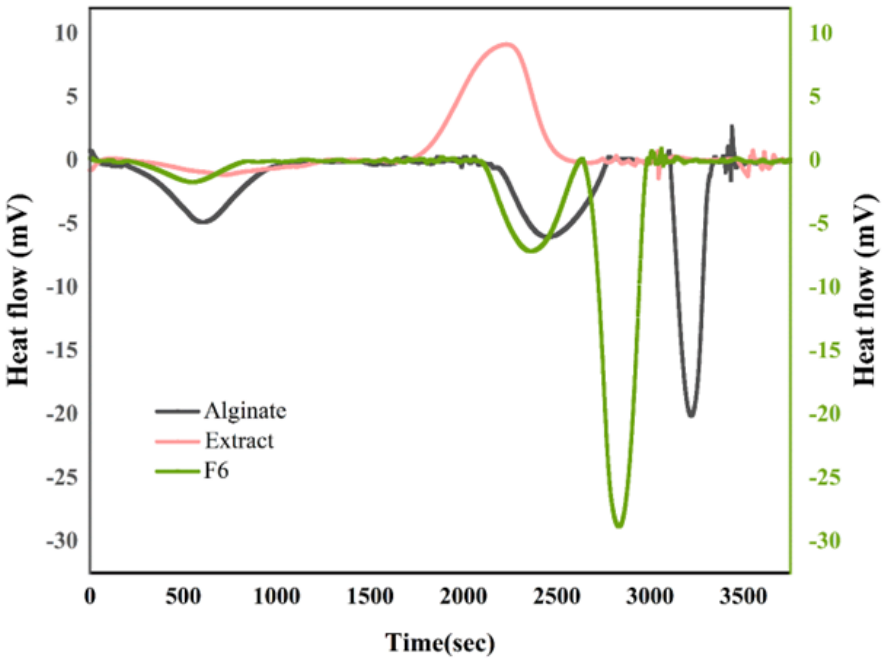

Figure 4. DSC thermograms of pure sodium alginate and *M. officinalis*-loaded encapsulated formulation prepared under selected conditions (115 °C, 4 bar, and 100 cm^3/s), showing characteristic thermal transitions including moisture loss, glass transition, and polymer decomposition.

https://doi.org/10.57647/pibm.2026.152604

processing in food and pharmaceutical applications, and supports the suitability of formulation F6 as a stable carrier for *M. officinalis* polyphenols in thermally processed food and nutraceutical products.

3.8 Alginate hydrogel swelling study

The swelling behavior of hydrogels is evaluated by the absorption of fluid, driven by the osmotic pressure gradient between the polymeric network and the surrounding medium. This phenomenon is typically quantified by measuring temporal changes in hydrogel mass [45]. In this study, the swelling capacity of the pure sodium alginate hydrogel and the extract-loaded system (F6, selected as the superior formulation) was assessed under simulated gastric conditions (pH 1.2). The swelling index was determined to be 1.89 ± 0.31 for the pure hydrogel and 1.78 ± 0.20 for the extract-loaded hydrogel. The reduced swelling observed in the extract-loaded system is attributed to increased matrix densification. This densification arises from hydrogen bonding interactions between alginate chains and the hydroxyl/carboxyl groups of phenolic compounds, which restricts water penetration into the network. Furthermore, swelling behavior is intrinsically pH-dependent; under acidic conditions, the protonation of carboxyl groups promotes intermolecular hydrogen bonding, leading to polymer chain contraction and reduced fluid uptake. These results highlight the influence of both environmental pH and hydrogel composition on swelling dynamics, parameters that are critical for the desig of alginate-based carriers for controlled drug delivery [26, 45].

3.9 Release behavior of *M. officinalis* extract from alginate encapsulated materials

The *in vitro* release kinetics of *M. officinalis* extract from the selected alginate nanoscale encapsulated materials (formulated at an inlet temperature of 115 °C, an atomizer pressure of 4 bar, and airflow rate of 100 cm^3/s) were investigated in SGF (pH 1.2) and SIF (pH 6.8) (Fig. 5). The encapsulated colloids displayed a pH-responsive release profile characteristic of polymeric carrier system. Under acidic conditions (pH 1.2), a biphasic release pattern was observed. An initial burst release (6.57% within 15 min) was attributed to the rapid desorption and dissolution of surface-bound phenolic compounds, followed by a slower diffusion-controlled phase (15.87% at 90 min). A slight decline in the detected concentration after 120 min was likely associated with the degradation of phenolic compounds in the highly acidic environment. In contrast, the release in SIF was rapid and nearly complete, with approximately 83% of the extract released within 15 min and ~ 100% within 30 min. This accelerated release rate was driven by ionization of the alginate carboxyl groups at a neutral pH, which promoted rapid matrix swelling and facilitated solvent diffusion [46, 47].

The underlying release mechanism is fundamentally tied to the pKa range (3.5 – 4.4) of carboxyl groups of alginates. In acidic conditions (below the pKa), the protonation of carboxyl groups (–COOH) reduces the charge density along the polymer backbone. This lack of electrostatic repulsion causes the matrix to remain contracted, thereby hindering fluid ingress and slowing the release of the encapsulated core. Conversely, in neutral or weakly alkaline conditions (above the pKa), ionization

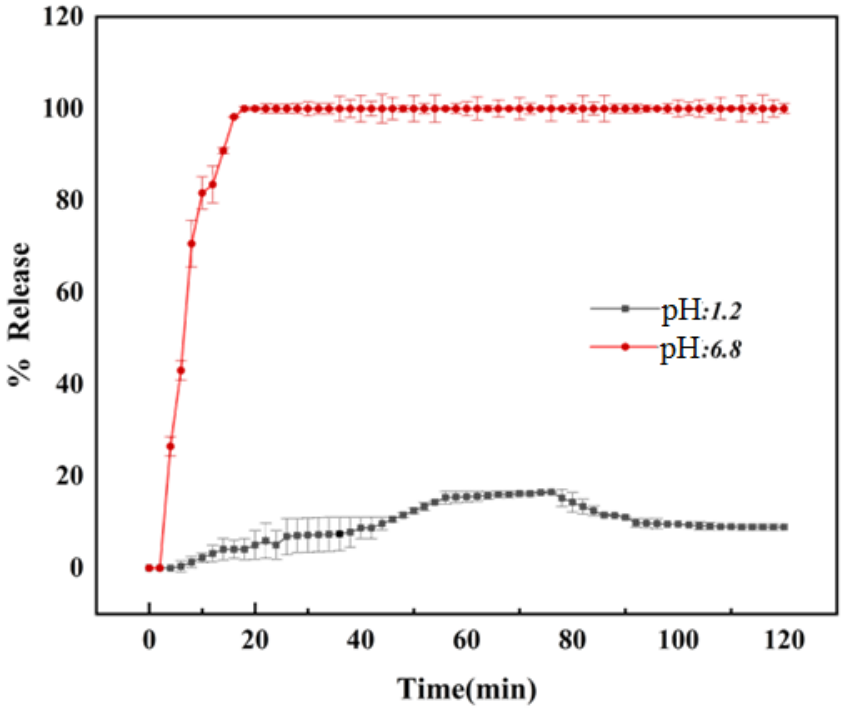

Figure 5. Cumulative release profile of *M. officinalis* extract from sodium alginate encapsulated materials under simulated gastric (pH 1.2) and intestinal (pH 6.8) conditions. Release was minimal in acidic medium (< 20% at 120 min) but rapid and nearly complete in intestinal medium (~ 100% within 30 min). Data represent mean ± SD (n = 3).

https://doi.org/10.57647/pibm.2026.152604

of these functional groups to carboxylate ions (–COO^-) generates strong electrostatic repulsion between adjacent polymer chains, leading to extensive structural swelling, matrix relaxation, and faster release. This pH- dependent swelling and contraction cycle effectively enable the alginate matrix to protect the sensitive phenolic compounds in the acidic gastric environment, while ensuring their rapid and targeted release in the neutral intestinal environment, thereby enhancing their potential bioavailability [47]. This behavior is consistent with established release models in which alginate networks undergo minimal hydration in gastric fluids but experience substantial swelling and erosion in intestinal fluids.

3.10 Docking studies and MD simulation

To obtain a mechanistic understanding of the encapsulation process at the atomic level, a combined computational approach utilizing molecular docking and MD simulations was employed. Given the macroscopic, amorphous, and highly flexible nature of alginate chains, modeling the entire polymer is computationally prohibitive and physically unrealistic. Therefore, a short sequence (comprising units B3, A4, B5, A6, and B7) was utilized as a representative structural model of the polymer backbone. This hierarchical computational strategy, employing molecular docking to establish the initial thermodynamically favorable host-guest coordinates, followed by MD simulations to evaluate the dynamic flexibility of the system, is a robust and well-documented method for elucidating entrapment mechanisms within complex biopolymer networks [48].

Based on this rationale, molecular docking and MD simulations were performed to explore the binding affinity between rosmarinic acid (the major phenolic marker of *M. officinalis*) and the representative alginate polymer. As illustrated in figure 6, rosmarinic acid, characterized by two aromatic rings and functional hydroxyl and carboxyl groups, showed a strong affinity for the alginate chains. Key interactions driving this complexation included hydrogen bonding between the ligand and the hydroxyl and carboxyl groups of alginates, hydrophobic contacts with nonpolar regions of the matrix, and electrostatic interactions with sodium ions in the polymer environment. The alginate units (B3, A4, B5, A6, and B7) formed a spatially stable complex with rosmarinic acid in an aqueous solution, further stabilized by the surrounding water molecules and sodium ions. These computational observations strongly support the experimental findings and highlight the molecular basis for the efficient encapsulation and stable retention of the extract within the matrix.

To assess structural stability, a 30-ns MD simulation was performed using the docked conformation as the starting structure. As shown in figure 7, the root-mean-square deviation (RMSD) profile indicated that rosmarinic acid maintained low fluctuations (1.5–2.5 Å), suggesting minimal conformational changes and stable binding within the alginate matrix. The representative alginate chain exhibited an initial RMSD rise to ~ 8 – 11 Å within the first few nanoseconds, reflecting expected structural rearrangement, followed by stabilization with moderate fluctuations. This behavior is highly typical of large flexible biopolymers. The polymer–ligand complex followed a similar RMSD pattern (8 – 12 Å), showing that ligand binding did not significantly disrupt the fundamental polymer conformation. The slightly higher fluctuations observed in the complex likely arose from continuous, dynamic intermolecular interactions between the polymer and ligand. Overall, these findings confirm that the rosmarinic acid–alginate complex remains structurally stable under the simulated conditions. The ligand stayed firmly bound, while the polymer maintained its integrity

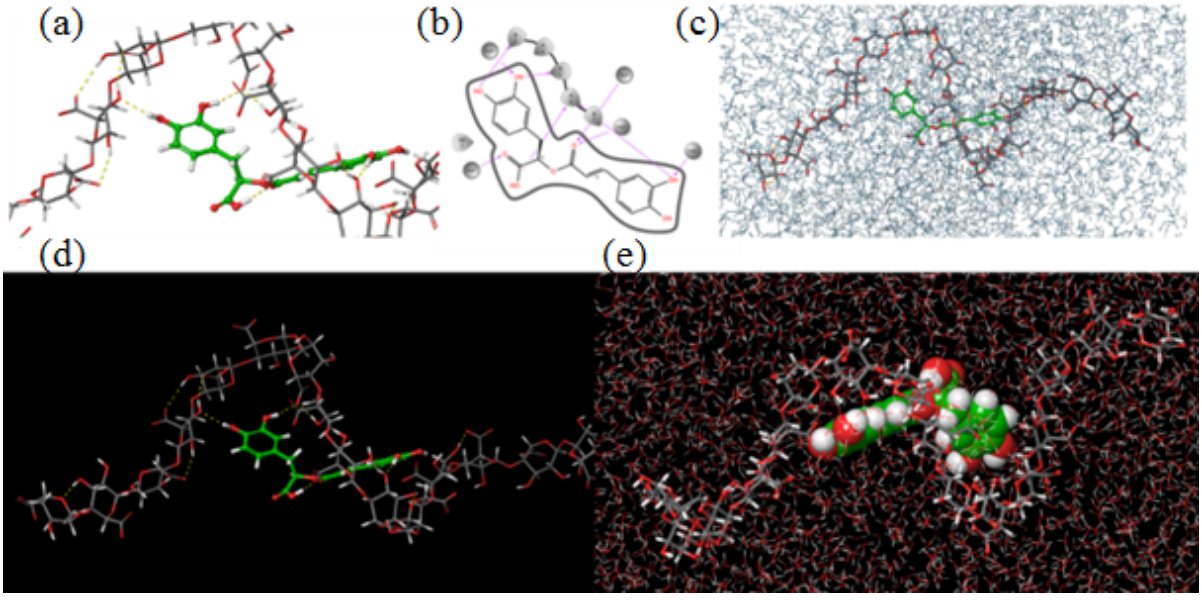

Figure 6. Molecular interactions between rosmarinic acid and the representative alginate polymer: (a) 3D binding configuration showing hydrogen bonds, hydrophobic contacts, and surrounding water molecules; (b) 2D interaction diagram depicting key residues and ionic contacts; (c–e) dynamic conformations of the rosmarinic acid–alginate complex in aqueous environment.

https://doi.org/10.57647/pibm.2026.152604

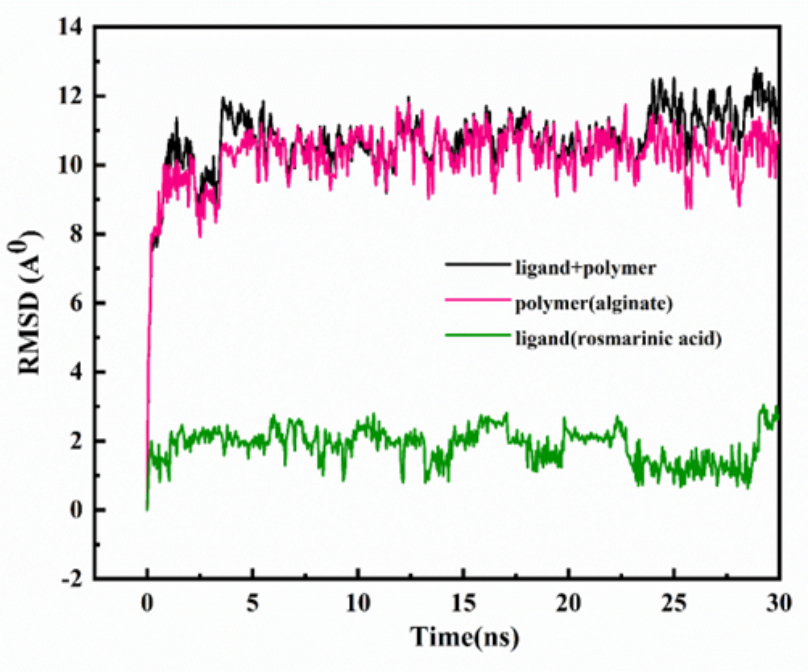

Figure 7. RMSD profiles of rosmarinic acid (green), alginate polymer (pink), and their complex (black) during a 30-ns MD simulation. The ligand remained structurally stable (1.5 – 2.5 Å fluctuations), while the polymer and complex showed initial rearrangements followed by stabilization at equilibrium.

after initial reorganization, computationally supporting the potential of this encapsulation system for stable and controlled release.

3.11 Stability assessment of encapsulated colloids produced by nano spray drying

A continuous evaluation of rosmarinic acid content across all formulations over a six-month storage period revealed a gradual decline, indicative of partial degradation under the tested conditions (Table 5). As demonstrated by the data, formulation F7 exhibited the highest percentage of retention, indicating superior stability and protection of the encapsulated compound. However, formulation F6 was ultimately identified as the most favorable and practical system overall. While F6 retained approximately 77% of its content, it possessed the highest initial loading capacity of rosmarinic acid (1.3 µg/mg). Consequently, despite the marginal difference in degradation percentages, F6 maintained the highest absolute mass of the intact bioactive compound at the end of the six-month storage period, making it the most efficient delivery vehicle. Furthermore, formulations processed at higher inlet temperatures, such as F10 (165 °C), displayed greater losses, emphasizing the critical need for moderate drying conditions to preserve heat-sensitive polyphenols. Particle size also influenced stability, with intermediate sizes (e.g., F6, ~ 620 nm) providing a highly effective physical barrier against environmental stressors. Overall, F6, produced under moderate thermal and pressure conditions, achieved the most favorable stability profile, underscoring the critical role of spray drying parameters in maintaining bioactive compound integrity during storage.

Table 5. The content of Rosmarinic acid (mg/g powder) in encapsulated colloids at day 1 and 180 days at storage.

code	Day 1	Day 180	Retain TPC (%)
F1	0.4 ± 0.01^{cd}	0.2 ± 0.01^{d}	50.00
F2	0.7 ± 0.04^{b}	0.4 ± 0.01^{b}	57.10
F3	0.4 ± 0.08^{cd}	0.3 ± 0.06^{c}	75.00
F4	0.4 ± 0.04^{cd}	0.0 ± 0.0^{f}	0.00
F5	0.5 ± 0.02^{c}	0.3 ± 0.02^{c}	60.00
F6	1.3 ± 0.01^{a}	1.2 ± 0.01^{a}	92.30
F7	0.2 ± 0.05^{e}	0.2 ± 0.01^{d}	100.00
F8	0.5 ± 0.03^{c}	0.1 ± 0.01^{e}	20.00
F9	0.4 ± 0.01^{cd}	0.2 ± 0.02^{d}	50.00
F10	0.3 ± 0.01^{de}	0.1 ± 0.01^{e}	33.30

"Retained TPC" is calculated as the percentage of total phenolic content retained, aiming for a concise comparison between the developed formulations after 180 days (6 months) under storage conditions. Different letters in same column indicate significant differences by Tukey's HSD test ($p < 0.05$).

3.12 Stability assessment of formulation F6 using DLS and zeta potential analysis

The physical stability of formulation F6 was evaluated over a 30-day period using DLS and zeta potential analysis (Table 6). The hydrodynamic diameter of the particles remained highly stable, ranging minimally from 841.56 ± 0.06 to 866.74 ± 0.02 nm, indicating the absence of significant aggregation or structural degradation over time. Furthermore, PDI remained consistently low (0.2 – 0.3), confirming a narrow and uniform size distribution. A slight decrease in PDI observed at day 10 suggests a

https://doi.org/10.57647/pibm.2026.152604

transient improvement in size homogeneity, likely due to minor matrix equilibration. The zeta potential values were moderately negative (−19.25 ± 0.78 to −20.85 ± 3.0 mV), providing sufficient electrostatic repulsion between the particles to effectively prevent aggregation. Taken together, these results demonstrate that formulation F6 retains its physicochemical integrity and colloidal stability for at least one month, highlighting its suitability as a robust bioactive delivery system for pharmaceutical and nutraceutical applications.

Table 6. Physical stability parameters of the formulation F6 over 30 days of storage.

Time (day)	DLS (nm)	PDI	Zeta Potential (mV)
0	862.8 ± 11.4[a]	0.3 ± 0.05[a]	−19.75 ± 0.05[a]
10	820.6 ± 6.0[a]	0.2 ± 0.02[a]	−20.85 ± 2.90[a]
20	866.7 ± 17.8[a]	0.2 ± 0.05[a]	−20.30 ± 2.70[a]
30	841.6 ± 11.59[a]	0.2 ± 0.04[a]	−19.25 ± 0.50[a]

Different letters in same column indicate significant differences by the Tukey's HSD test ($p < 0.05$)

4. Conclusion

This study demonstrated the successful encapsulation of *M. officinalis* phenolic compounds within sodium alginate nanoscale encapsulated materials produced by spray drying. Process parameters, including inlet air temperature, atomizer pressure, airflow rate, and feed concentration, were systematically screened to evaluate their effects on particle characteristics, antioxidant activity, and release behavior. The most favorable formulation (115 °C, 4 bar, 100 cm^3/s) yielded encapsulated materials (~ 620 nm, PDI: 0.3) with high encapsulation efficiency (88.65 ± 0.57%) alongside a biphasic, pH-responsive release profile. Complementary analytical and computational analyses (FTIR, DSC, and molecular docking/MD simulation) confirmed robust intermolecular interactions between the phenolic compounds and the alginate matrix, which improved structural stability and facilitated controlled release.

Crucially, the developed formulation holds significant practical relevance for food, nutraceutical, and pharmaceutical applications. By utilizing sodium alginate, a generally recognized as safe (GRAS), biocompatible polysaccharide, this encapsulation system effectively shields the sensitive *M. officinalis* polyphenols from premature thermal degradation during processing and harsh gastric conditions upon ingestion. Furthermore, the pH-responsive nature of the alginate matrix ensures targeted release predominantly within the intestinal environment, thereby maximizing the potential bioavailability and therapeutic efficacy of the botanical payload. These findings provide scalable, mechanistic guidelines for integrating natural polyphenols into functional products. While this work establishes a robust foundation through *in vitro* and computational models, future studies focusing on comparative carrier systems, extended MD simulations, and *in vivo* evaluations will further enhance translational relevance and practical application of this targeted delivery system.

Acknowledgment

The authors gratefully acknowledge the financial and logistical support provided by the Research Council of Shahid Beheshti University. Special thanks are extended to Ms. Mahshad Shariari for her valuable contribution in performing the molecular simulations.

Authors contributions

Leila Bagherpour: Investigation, Methodology, Formal analysis, Validation, Writing original draft. Samad Nejad Ebrahimi: Conceptualization, Investigation, Software, Data curation, Formal analysis, Methodology, Visualization, Validation, Writing original draft, Writing—review and editing, Resources, Funding acquisition, Project administration. Hasan Rafati: Formal analysis, Visualization, Writing review and editing. Marzieh Omrani: Validation, Writing review and editing.

Availability of data and materials

The datasets generated during and/or analyzed during the current study are available from the corresponding author on reasonable request.

Conflict of interests

The authors declare that they have no known competing financial interests or personal relationships that could have appeared to influence the work reported in this paper.

References

1. Pop CR, Zahan M, Crisan I, Stefan R, Varban D, Gál E, Varban R, Rotar AM, Coldea S, and Olar L. *Melissa officinalis* L. hydro-alcoholic extract inhibits anxiety and depression through prevention of central oxidative stress and apoptosis. Experimental Physiology 2020; 105:707–20. DOI: 10.1113/EP088254
2. Ghazizadeh J, Hamedeyazdan S, Torbati M, Farajdokht F, Fakhari A, Mahmoudi J, Araj-Khodaei M, and Sadigh-Eteghad S. *Melissa officinalis* L. hydro-alcoholic extract inhibits anxiety and depression through prevention of central oxidative stress and apoptosis. Experimental Physiology 2020; 105:707–20. DOI: 10.1113/EP088254
3. Encalada MA, Hoyos KM, Rehecho S, Berasategi I, Ciriano MGI de, Ansorena D, Astiasarán I, Navarro-Blasco I, Cavero RY, and Calvo MI. Antiproliferative Effect of *Melissa officinalis* on Human Colon Cancer Cell Line. Plant Foods for Human Nutrition 2011; 66:328–34. DOI: 10.1007/s11130-011-0256-y
4. Ghiulai R, Avram S, Stoian D, Pavel IZ, Coricovac D, Oprean C, Vlase L, Farcas C, Mioc M, Minda D, Motoc A, Szuhanek C, Danciu C, Soica C, and Sima L. Lemon Balm Extracts Prevent Breast Cancer Progression *In Vitro* and *In Ovo* on Chorioallantoic Membrane Assay. Evidence-Based

Complementary and Alternative Medicine: ECAM 2020; 2020:6489159. DOI: 10.1155/2020/6489159

5. Astani A, Reichling J, and Schnitzler P. *Melissa officinalis* extract inhibits attachment of herpes simplex virus *in vitro*. Chemotherapy 2012; 58:70–7. DOI: 10.1159/000335590
6. Pereira RP, Fachinetto R, Souza-Prestes A de, Puntel RL, Silva GNS da, Heinzmann BM, Boschetti TK, Athayde ML, Bürger ME, Morel AF, Morsch VM, and Rocha JBT. Antioxidant effects of different extracts from *Melissa officinalis*, Matricaria recutita and Cymbopogon citratus. Neurochemical Research 2009; 34:973–83. DOI: 10.1007/s11064-008-9861-z
7. Gurbuz P, Martinez A, Perez C, Martínez-González L, Goger F, and Ayran-Çolak I. Potential anti-Alzheimer effects of selected Lamiaceae plants through polypharmacology on glycogen synthase kinase-3β, β-secretase, and casein kinase 1δ. Industrial Crops and Products 2019; 138:111431. DOI: 10.1016/j.indcrop.2019.05.080
8. Araújo SG, Lima WG, Amaral-Pinto ME, Morais MI, Pereira-de N, Johann S, Rosa CA, and Alves-Rodrigues L. Pharmacological prospection *in-vitro* of Lamiaceae species against human pathogenic fungi associated to invasive infections. Biocatalysis and Agricultural Biotechnology 2019; 21:101345. DOI: 10.1016/j.bcab.2019.101345
9. Shin Y, Lee D, Ahn J, Lee M, Shin SS, and Yoon M. The herbal extract ALS-L1023 from *Melissa officinalis* reduces weight gain, elevated glucose levels and β-cell loss in Otsuka Long-Evans Tokushima fatty rats. Journal of Ethnopharmacology 2021; 264:113360. DOI: 10.1016/j.jep.2020.113360
10. Pan F, Liu X, Qiao M, Liu J, Pang Y, Zhang M, and Yu W. Innovative composite systems for enhancing plant polyphenol stability and bioavailability. Food Sci. Biotechnol. 2025; 34. DOI: 10.1007/s10068-024-01753-3
11. Stini E and Tsimogiannis D. The Valorisation of Melissa officinalis Distillation By-Products for the Production of Polyphenol-Rich Formulations. 2024. DOI: 10.3390/molecules29020377
12. Hay TO, Nastasi JR, Prakash S, and Fitzgerald MA. Comparison of Gidyea gum, gum Arabic, and maltodextrin in the microencapsulation and colour stabilisation of anthocyanin-rich powders using freeze-drying and spray-drying techniques. Food Hydrocolloids 2025; 163:111023. DOI: 10.1016/j.foodhyd.2024.111023
13. Fathi F, Ebrahimi SN, Pereira DM, Estevinho BN, and Rocha F. Microencapsulation of Enriched Extracts of Two Satureja Species by Spray Drying, Evaluation of the Controlled Release Mechanism and Cytotoxicity. Pharmaceutical Sciences 2022; 28:145–55. DOI: 10.34172/PS.2021.54
14. Pinón-Balderrama CI, Leyva-Porras C, Terán-Figueroa Y, Espinosa-Solís V, Salas C Álvarez, and Saavedra-Leos MZ. Encapsulation of active ingredients in food industry by spray-drying and nano spray-drying technologies. Processes 2020; 8. DOI: 10.3390/PR8080889
15. Bürki K, Jeon I, Arpagaus C, and Betz G. New insights into respirable protein powder preparation using a nano spray dryer. International Journal of Pharmaceutics 2011; 408:248–56. DOI: 10.1016/j.ijpharm.2011.02.012
16. Sentkowska A, Biesaga M, and Pyrzynska K. Polyphenolic Composition and Antioxidative Properties of Lemon Balm (*Melissa officinalis* L.) Extract Affected by Different Brewing Processes. International Journal of Food Properties 2015; 18:2009–14. DOI: 10.1080/10942912.2014.960932
17. Rajabi H and Razavi SMA. Co-encapsulation of saffron petal and Stachys schtschegleevii extracts via complex coacervation and graphene oxide-assisted spray drying for co-delivery and stability enhancement. LWT 2025; 223:117705. DOI: 10.1016/j.lwt.2025.117705
18. Keawchaoon L and Yoksan R. Preparation, characterization and *in vitro* release study of carvacrol-loaded chitosan nanoparticles. Colloids and Surfaces B: Biointerfaces 2011; 84:163–71. DOI: 10.1016/j.colsurfb.2010.12.031
19. Zokti JA, Sham-Baharin B, Mohammed AS, and Abas F. Green Tea Leaves Extract: Microencapsulation, Physicochemical and Storage Stability Study. Molecules (Basel, Switzerland) 2016; 21. DOI: 10.3390/molecules21080940
20. Sarma N, Upton R, Rose U, Guo D, Marles R, Khan I, and Giancaspro G. Pharmacopeial standards for the quality control of botanical dietary supplements in the United States. Journal of Dietary Supplements 2023; 20:485–504. DOI: 10.1080/19390211.2021.1990171
21. Najafi-Soulari S, Shekarchizadeh H, and Kadivar M. Encapsulation optimization of lemon balm antioxidants in calcium alginate hydrogels. Journal of Biomaterials Science 2016; 27:1631–44. DOI: 10.1080/09205063.2016.1226042
22. Swamy TMM, Ramaraj B, and Lee JH. Sodium Alginate and Its Blends with Starch: Thermal and Morphological Properties. Journal of Biomaterials Science 2008. DOI: 10.1002/app
23. Markus K, Kirschbaum T, Metzsch-Zilligen E, and Pfaendner R. Processing stability and radical scavenging efficiency of novel biobased stabilizers: Insights from long-term extrusion and DPPH assays. Polymer Degradation and Stability 2025; 233:111162. DOI: 10.1016/j.polymdegradstab.2024.111162

24. Saadatidizaji Z, Sohrabi N, Mohammadi R, and Amini-Fazl MS. Tetracycline hydrochloride loaded-alginate based nanoparticle-hydrogel beads for potential wound healing applications: *In vitro* drug delivery, release kinetics, and antibacterial activity. International Journal of Biological Macromolecules 2024; 264:130653. DOI: 10.1016/j.ijbiomac.2024.130653

25. Deng R, Mars M, VanDer-Sman RGM, Smeets PAM, and Janssen AEM. The importance of swelling for *in vitro* gastric digestion of whey protein gels. Food Chemistry 2020; 330:127182. DOI: 10.1016/j.foodchem.2020.127182

26. Patel N, Lalwani D, Gollmer S, Injeti E, Sari Y, and Nesamony J. Development and evaluation of a calcium alginate based oral ceftriaxone sodium formulation. Progress in Biomaterials 2016; 5:117–33. DOI: 10.1007/s40204-016-0051-9

27. Gayibova SN, Ivanivsová E, Árvay J, Hŕstková M, Slávik M, Petrová J, Hleba L, Tóth T, Kavcániová M, and Aripov TF. *In Vitro* Screening Of Antioxidant And Antimicrobial Activities Of Medicinal Plants Growing In Slovakia. Journal of Microbiology, Biotechnology and Food Sciences 2019. DOI: 10.15414/jmbfs.2019.8.6.1281-1289

28. Fierascu I, Georgiev MI, Ortan A, Fierascu RC, Avramescu SM, Ionescu D, Sutan A, Brinzan A, and Ditu LM. Phyto-mediated metallic nanoarchitectures via *Melissa officinalis* L.: synthesis, characterization and biological properties. Scientific Reports 2017; 7:12428. DOI: 10.1038/s41598-017-12804-7

29. Tülek Z, Alaşalvar H, Başyiğit B, Berktas S, Salum P, Erbay Z, Telci I, and Çam M. Extraction optimization and microencapsulation of phenolic antioxidant compounds from lemon balm (*Melissa officinalis* L.): Instant soluble tea production. Journal of Food Processing and Preservation 2020. DOI: 10.1111/jfpp.14995

30. Zhang L, Tang P, Li S, Wang X, and Zong W. Sodium alginate-based wall materials microencapsulated Lactobacillus plantarum CICC 20022: characteristics and survivability study. Food Science and Biotechnology 2022; 31:1463–72. DOI: 10.1007/s10068-022-01134-8

31. Lemmadi S, Dumas E, Adoui F, Agusti G, Vessot-Crastes S, Medfai W, and Gharsallaoui A. Spray-Drying Microencapsulation of Artemisia herba-alba Phenolic Extract: Physicochemical Properties, Structural Characterization, and Bioactivity. Molecules 2025; 30. DOI: 10.3390/molecules30193904

32. Arauzo B, González-Garcinuno A, Tabernero A, Lobera MP, Santamaria J, and Martín-DelValle EM. Tuning Alginate Microparticle Size via Atomization of Non-Newtonian Fluids. Materials 2021; 14. DOI: 10.3390/ma14247601

33. Eijkelboom NM, Van-Boven AP, Siemons I, Wilms PFC, Boom RM, Kohlus R, and Schutyser MAI. Particle structure development during spray drying from a single droplet to pilot-scale perspective. Journal of Food Engineering 2023; 337:111222. DOI: 10.1016/j.jfoodeng.2022.111222

34. Tontul I and Topuz A. Spray-drying of fruit and vegetable juices: Effect of drying conditions on the product yield and physical properties. Trends in Food Science & Technology 2017; 63:91–102. DOI: 10.1016/j.tifs.2017.03.009

35. Ziaee A, Albadarin AB, Padrela L, Femmer T, O'Reilly E, and Walker G. Spray drying of pharmaceuticals and biopharmaceuticals: Critical parameters and experimental process optimization approaches. European Journal of Pharmaceutical Sciences: Official Journal of the European Federation for Pharmaceutical Sciences 2019; 127:300–18. DOI: 10.1016/j.ejps.2018.10.026

36. Sun X, Cameron RG, and Bai J. Effect of spray-drying temperature on physicochemical, antioxidant and antimicrobial properties of pectin/sodium alginate microencapsulated carvacrol. Food Hydrocolloids 2020; 100. DOI: 10.1016/j.foodhyd.2019.105420

37. Judson-King C. Spray Drying: Retention of Volatile Compounds Revisited. Drying Technology 1995; 13:1221–40. DOI: 10.1080/07373939508917018

38. Stefanescu BE, Nemes SA, Teleky BE, Calinoiu LF, Mitrea L, Martau GA, Szabo K, Mihai M, Vodnar DC, and Crisan G. Microencapsulation and Bioaccessibility of Phenolic Compounds of Vaccinium Leaf Extracts. Antioxidants (Basel, Switzerland) 2022; 11. DOI: 10.3390/antiox11040674

39. Zhang J, Hamadou AH, Chen C, and Xu B. Encapsulation of phenolic compounds within food- grade carriers and delivery systems by pH-driven method: a systematic review. Crit. Rev. Food Sci. Nutr. 2023; 63:4153–4174. DOI: 10.1080/10408398.2021.1998761

40. Fang Z and Bhandari B. Encapsulation of polyphenols – a review. Trends in Food Science & Technology 2010; 21:510–23. DOI: 10.1016/j.tifs.2010.08.003

41. Espíndola SP, Norder B, Koper GJM, and Picken SJ. The Glass Transition Temperature of Heterogeneous Biopolymer Systems. Biomacromolecules 2023; 24:1627–37. DOI: 10.1021/acs.biomac.2c01356

42. Russo R, Malinconico M, and Santagata G. Effect of Cross-Linking with Calcium Ions on the Physical Properties of Alginate Films. Biomacromolecules 2007; 8:3193–3197. DOI: 10.1021/bm700565h

43. Mourtzinos I, Papadakis S, and Igoumenidis P. Encapsulation of Melissa Officinalis leaf ' s active compounds in ü -cyclodextrin and modified starch. Ital. Oral Surg. 2011; 1:1679–1685. DOI: 10.1016/j.profoo.2011.09.248

44. Reddy-Obireddy S, Bellala S, Chintha M, Sake A, Marata-Chinna S, and Lai WF. Synthesis and properties of alginate-based nanoparticles incorporated with different inorganic nanoparticulate modifiers for enhanced encapsulation and controlled release of favipiravir. Arabian Journal of Chemistry 2023; 16:104751. DOI: 10.1016/j.arabjc.2023.104751

45. Zou Z, Zhang B, Nie X, Cheng Y, Hu Z, Liao M, and Li S. A sodium alginate-based sustained-release IPN hydrogel and its applications. RSC Advances 2020; 10:39722–30. DOI: 10.1039/d0ra04316h

46. Kamal S, Shoukat S, Rehman K, Malik S, Batool F, Ahsan A, and Akash MSH. pH-Responsive Inulin–Sodium Alginate Hydrogel Beads for Sustained Oral Delivery of Bacterial Serine Protease. Bioengineering 2026; 13:655. DOI: 10.3390/bioengineering13060655

47. Basu R and Noor A. Development of alginate-based encapsulation of enriched polyphenols from Desmodium gangeticum leaves: Characterization, stability, *in-vitro* release study and biological activities. Food Biosci. 2024; 61:104535. DOI: 10.1016/j.fbio.2024.104535

48. Shahriari M, Ebrahimi SN, Rahimi M, Khademian A, Ardekani MM, Alves RC, Oliveira MBPP, and Fathi F. pH-responsive chitosan/PVA-based fiber films with enhanced antioxidant and colorimetric response via pomegranate anthocyanin enrichment. Int. J. Biol. Macromol. 2025 :147164. DOI: 10.1016/j.ijbiomac.2025.147164